Hindawi Publishing Corporation
Journal of Nanoparticles
Volume 2015, Article ID 816982, 7 pages
http://dx.doi.org/10.1155/2015/816982

Research Article

Effect of Microbes on the Adsorption of Naphthalene by Graphene Oxide

Xiaoyu Li, Fengbo Li, and Lejin Fang

The School of Life Science and Environmental Science, Huangshan University, Huangshan 245041, China

Correspondence should be addressed to Fengbo Li; 0550-6732966@163.com

Received 27 February 2015; Revised 4 July 2015; Accepted 5 July 2015

Academic Editor: Ovidiu Ersen

The adsorption of naphthalene on graphene oxide (GO) nanosheets in presence of *Paecilomyces cateniannulatus* (*P. cateniannulatus*) was conducted by the batch techniques. The morphology and nanostructure of GO were characterized by SEM, TEM, FTIR, XPS, and Raman. The adsorption kinetics indicated that the adsorption of naphthalene on GO and GO + *P. catenlannulatus* can be satisfactorily fitted pseudo-first-order and pseudo-second-order kinetic model, respectively. *P. catenlannulatus* inhibited the adsorption of naphthalene on GO at pH < 4.0, whereas the increased adsorption was observed at pH > 4.0. The adsorption of naphthalene on GO and GO + *P. catenlannulatus* can be better fitted by Langmuir and Freundlich model, respectively. The change in the conformation of GO was responsible to the increased adsorption of naphthalene by SEM and TEM images. According to FTIR analysis, naphthalene was absorbed by the oxygen-containing functional groups of GO, especially for –COOH. The finding in the study provides the implication for the preconcentration and removal of polycyclic aromatic hydrocarbons from environment cleanup applications.

1. Introduction

Graphene oxide (GO), as the precursor of graphene, exhibits the large number of hydroxyl and epoxy groups in the plane and a small amount of carboxyl and carbonyl group at the edge [1–3]. Recently, it has been reported that GO displays the excellent adsorption performance for many organic contaminants, such as dyes [4–7], polychlorinated biphenyls (PCBs) [8–10], and polycyclic aromatic hydrocarbons (PAHs) [11–13]. Wang et al. [13] investigated that the high affinities of the PAHs to GO were attributed to the carboxyl groups attaching to the edges of GO. Recent studies have revealed that the hydrophilic GO solution can transfer into the natural aquatic environments, which causes greater environmental risks [14]. Therefore, understanding on the interaction between GO and microbes plays a vital role in evaluating the fate and transport of GO in the aquatic environments.

Paecilomyces cateniannulatus (P. cateniannulatus) is carnivorous fungi specialized in trapping and digesting nematodes, which has been extensively used to kill harmful nematodes by pathogenesis [15]. It is demonstrated that *P. catenlannulatus* also can be used as a promising adsorbent to remove heavy metals [16–21]. Li et al. [20] found that the maximum adsorption capacity of *P. catenlannulatus* calculated from Langmuir model was 140.85 mg/g for Hg(II). Such high affinity for heavy metals was attributed to a variety of oxygen-containing functional groups such as amine, phosphoryl, carboxyl, and hydroxyl groups [21]. However, to the author's knowledge, little information on the effect of *P. catenlannulatus* on the adsorption of organic contaminants is available.

The objectives of this study are to (1) synthesize GO nanosheets and characterize the microstructure of GO by scanning electron microscopy (SEM), transmission electron microscopy (TEM), Fourier transformed infrared (FTIR), X-ray photoelectron spectroscopy (XPS), and Raman techniques; (2) investigate the effect of *P. cateniannulatus* on the adsorption of naphthalene onto GO under various environmental conditions; (3) determine the interaction mechanism between naphthalene and GO + *P. cateniannulatus* by TEM and XPS. The paper highlights the molecular mechanisms and conformations that influence the adsorption of microbes onto graphene-based nanomaterials.

2. Experimental

2.1. Materials. Flake graphite (225 mesh, 99.8%) was purchased from Qingdao Tianhe Graphite Co., Ltd. The strain 13 of *P. catenlannulatus* was cultured from the microbiology laboratory of University of Huangshan, China, which was isolated from infected pupae of the lepidopteran *T. pityocampa* in NE China. All chemicals as analytical reagent were purchased from Sinopharm Chemical Reagent Co., Ltd.

2.2. Synthesis of GO. GO nanosheets were synthesized using a modified Hummers method [22]. Typically, 1.5 g flake graphite and 100 mL concentrated H_2SO_4 were poured into 500 mL round-bottom flask under vigorous stirring and ice-water bath conditions; then 6.0 g of $KMnO_4$ was slowly added into the aforementioned suspensions. The suspensions were vigorously stirred for one week at room temperature. Then 12 mL H_2O_2 (30 wt %) was added in the suspension, and the mixture was stirred for 2 hr at room temperature. After centrifugation at 23000 rpm for 60 min, the solid phase was dispersed using vigorous stirring and bath ultrasonication for 30 min at the power of 140 W. The centrifugation and ultrasonication were recycled for several times, and then the sample was rinsed with Milli-Q water until the solution was neutral. The few-layered GO was obtained by freeze-drying it in a vacuum tank overnight.

2.3. Characterization. The nanostructures of GO were synthesized by SEM (JSM-6700F field emission scanning electron microscope, JEOL), TEM (JEOL-2010 transmission electron microscope, Japan), FTIR (JASCO FT-IR 410 spectrophotometer) with the KBr pellet technology, and XPS (ESCALAB 250Xi XPS analyzer, Thermo Scientific) with monochromatic Al $K\alpha$ X-ray source ($h\nu$ = 1486.6 eV) at a vacuum below 10^{-7} Pa and Raman (LabRam HR Raman spectrometer, France) at 514.5 nm with Ar^+ laser. The samples used for the SEM and TEM observation were prepared by dropping the GO suspension on copper foil.

2.4. Batch Adsorption Experiments. The adsorption kinetics and isotherms of naphthalene onto GO in the presence and absence of *P. cateniannulatus* were conducted in PTFE screw cap vials sealed with aluminum foil at 293 K. The sorption kinetic studies and pH-dependent experiments were performed with an initial naphthalene concentration of 5.0 mg/L, and the solid-to-liquid ratio was 0.25 g/L. To reach the maximum adsorption performance, the initial concentration of naphthalene solution was obtained over wide ranging from 30 μg/L to 10.0 mg/L. After equilibrium (24 h), the naphthalene concentration in the supernatants was analyzed by an Agilent 1200 HPLC equipped with a fluorescence detector. The distribution adsorption coefficient (K_d, L/g) and sorption capacity (Q_e, mg/g) can be calculated by (1) and (2), respectively:

$$K_d = V \times \frac{\left(C_0 - C_{\text{eq}}\right)}{\left(C_{\text{eq}} \times m\right)}, \quad (1)$$

$$Q_e = V \times \frac{\left(C_0 - C_{\text{eq}}\right)}{m}, \quad (2)$$

where C_0 (mg/L) and C_{eq} (mg/L) are initial concentration and equilibrated concentration after sorption, respectively. m (g) and V (mL) are the mass of adsorbents and the volume of the suspension, respectively. All experimental data were the average of triplicate determinations and the error bars (within ±5%) were provided.

3. Results and Discussion

3.1. Characterization. The morphology and nanostructure of GO were characterized by SEM and TEM techniques. As shown in the SEM image of GO in Figure 1(a), GO displayed the aggregated nanosheets, which were consistent with previous studies [23–25]. The transparent and randomly accumulated with the wrinkles of GO was observed (Figure 1(c)). The BET specific surface area of GO was calculated to be 240 m^2/g, which was significantly lower than the theoretical data (approximately 2630 m^2/g) due to the incomplete exfoliation and aggregation [26]. The deconvolution of the C 1s peak of GO was shown in Figure 1(e). As illustrated in Figure 1(e), the main peaks at 284.7, 286.6, 287.9, and 289.8 eV were ascribed to the C–C, C–O, C=O, and O–C=O, respectively [27–29]. According to the XPS analysis, the contents of oxygen in GO and hydrogen were approximately 30.96 and 0.11 atomic %, respectively. In the Raman spectra (Figure 1(f)), two main peaks at 1350 (D band, the stretching vibration of sp^3 carbon atoms) and 1580 cm^{-1} (G band, the stretching vibration of sp^2 carbon atoms) were observed. The D and G band were related with the defects/disorders and first-order scattering of the E_{2g} mode, respectively [13, 30]. The intensity ratio of the D band and G band (I_D/I_G) of GO (0.83) was smaller than that reduced GO (1.13), which indicated the defects/disorders of GO nanosheets compared to reduced GO nanosheets [31, 32]. Based on the characteristic results, it was demonstrated that GO nanosheets presented a variety of oxygen-containing functional groups such as epoxy, carboxyl, carbonyl, and hydroxyl groups.

3.2. Adsorption Kinetics. Figure 2 showed the adsorption kinetics of naphthalene on GO and GO + *P. catenlannulatus*. As shown in Figure 2(a), the adsorption of naphthalene on GO significantly increased with increasing reaction times from 0 to 3 h; then high-level adsorption was observed. However, the increased adsorption of naphthalene on GO + *P. catenlannulatus* was observed with increasing reaction times. It should be noted that *P. catenlannulatus* facilitated the adsorption of naphthalene on GO. The adsorption kinetics of naphthalene on GO and GO + *P. catenlannulatus* were fitted by pseudo-first-order and pseudo-second-order kinetic models. Their linear forms of pseudo-first-order [33] and pseudo-second-order kinetic models [34] were given in (3) and (4), respectively:

$$\ln\left(q_e - q_t\right) = \ln q_e - k_f \times t, \quad (3)$$

$$\frac{t}{q_t} = \frac{1}{\left(k_s \times q_e{}^2\right)} + \frac{t}{q_e}, \quad (4)$$

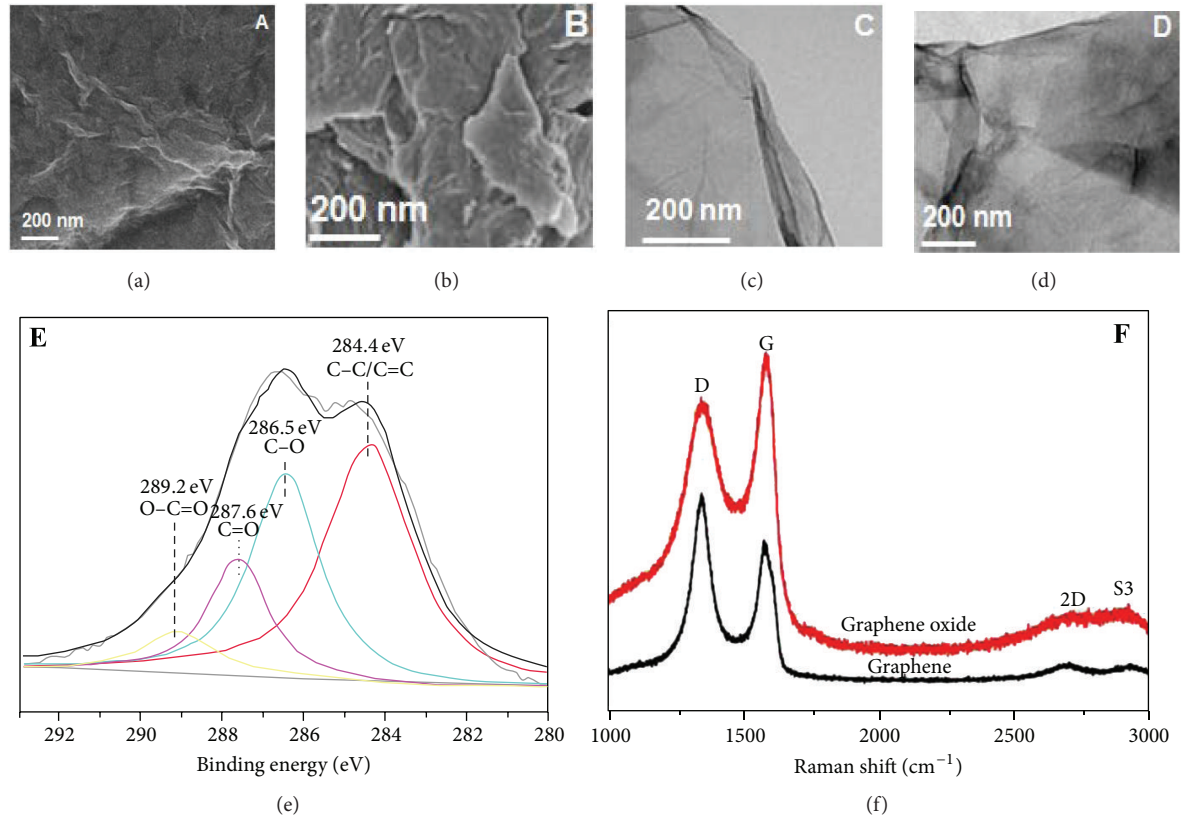

FIGURE 1: The characterization of GO (a) and (b) SEM images of GO before and after adsorption; (c) and (d) TEM images of GO before and after adsorption; (e) XPS (C 1s) spectra; (f) Raman spectra.

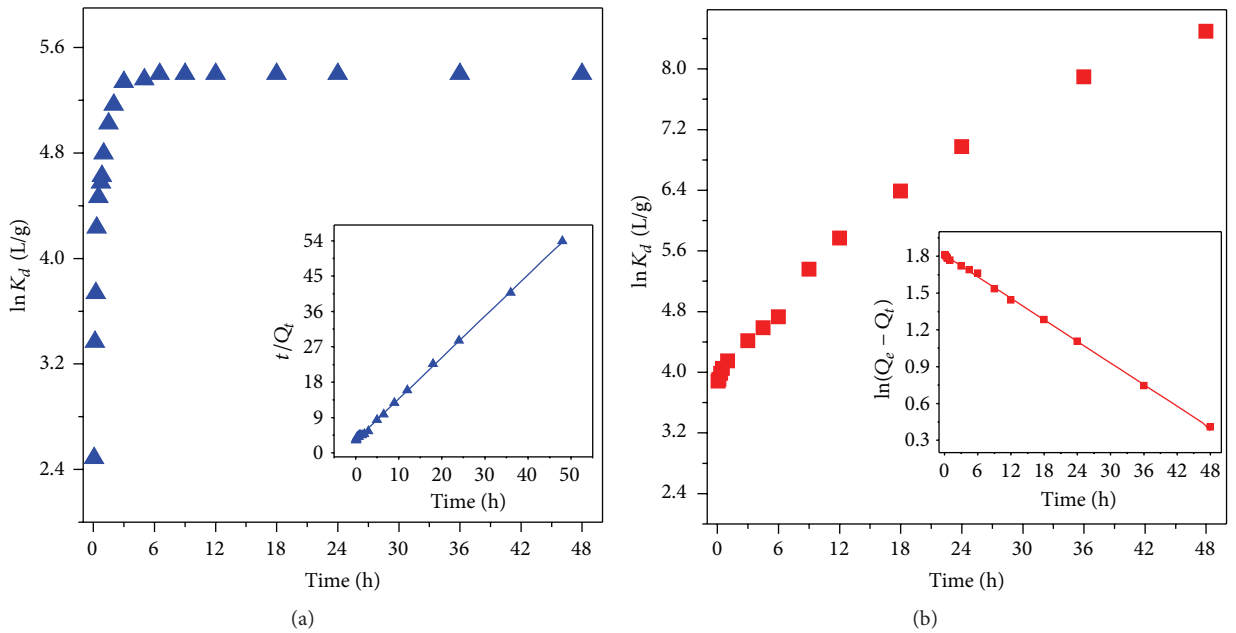

FIGURE 2: The adsorption kinetics of naphthalene on GO (a) and GO + *P. cateniannulatus* (b), pH 5.0, I = 0.01 mol/L $NaClO_4$, C_{NAP} = 5.0 mg/L, m/v = 0.25 g/L, and T = 293 K.

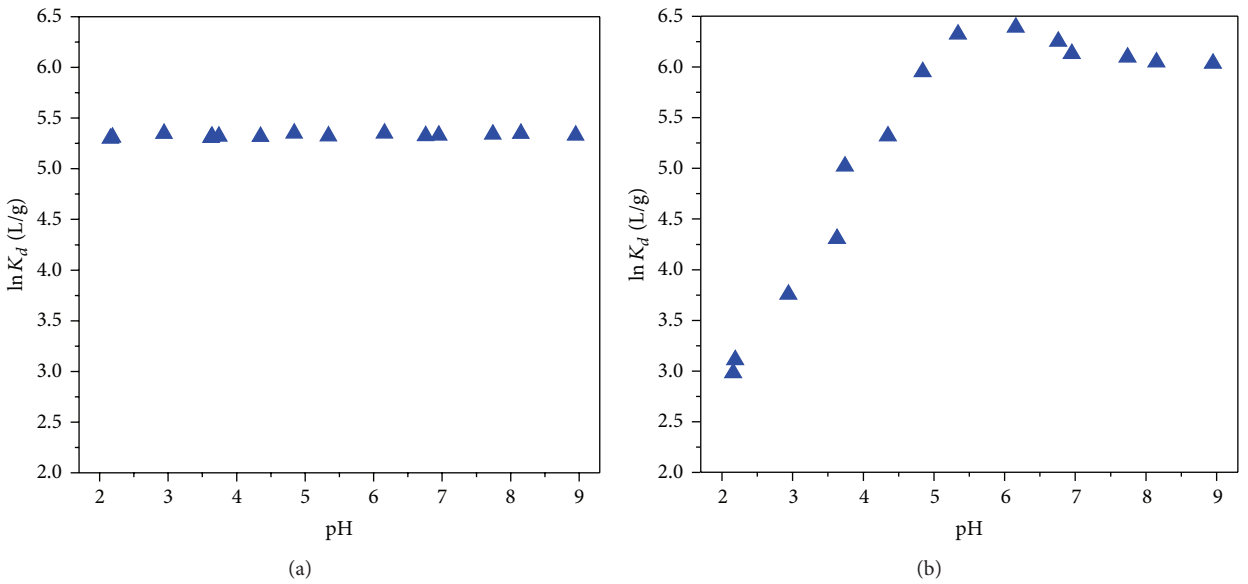

Figure 3: The effect of pH on naphthalene adsorption onto GO (a) and GO + *P. cateniannulatus* (b), I = 0.01 mol/L $NaClO_4$, C_{NAP} = 5.0 mg/L, m/v = 0.25 g/L, and T = 293 K.

Table 1: Kinetic parameters of naphthalene adsorption on GO and GO + *P. cateniannulatus*.

Parameters	GO	GO + *P. cateniannulatus*
Pseudo-first-order model		
k_f (/h)	0.0054	0.0293
q_e (mg/g)	5.414	6.10
R^2	0.2545	0.9993
Pseudo-second-order model		
k_s (g/(mg·h))	0.345	0.4813
q_e (mg/g)	0.9497	0.0484
R^2	0.9996	0.9774

where q_e and q_t (mg/g) are the amount of naphthalene adsorbed at equilibrium and at time t, respectively. k_f and k_s are the pseudo-first-order and pseudo-second-order kinetic rate constant, respectively. As shown in inset in Figures 2(a) and 2(b), it was observed that the adsorption of naphthalene on GO and GO + *P. catenlannulatus* can be satisfactorily fitted pseudo-second-order and pseudo-first-order kinetic model (correlation coefficient $R^2 > 0.999$), respectively (Table 1). The results from adsorption kinetics indicated that *P. catenlannulatus* significantly influenced the adsorption mechanism of naphthalene on GO nanosheets.

3.3. pH Effect. The effect of pH on naphthalene adsorption by GO and GO + *P. catenlannulatus* was shown in Figure 3. As shown in Figure 3(a), the adsorption of naphthalene on GO was independent of ionic strength, whereas the naphthalene adsorption on GO + *P. catenlannulatus* significantly increased with increasing pH from 2.0 to 5.0 (Figure 3(b)). Sun et al. [12] also found that the adsorption of naphthalene on GO was independent of pH; therefore the authors demonstrated that pore filling and flat surface adsorption dominated the adsorption of naphthalene on GO. The high-level adsorption of naphthalene on GO + *P. catenlannulatus* was also observed at pH 5.0–6.0; then adsorption of naphthalene on GO + *P. catenlannulatus* slightly decreased at pH > 6.5. It should be noted that *P. catenlannulatus* inhibited the adsorption of naphthalene on GO at pH < 4.0, whereas the *P. catenlannulatus* facilitated the adsorption of naphthalene on GO at pH > 4.0. The inhibited adsorption of naphthalene on GO in the presence of *P. catenlannulatus* at pH < 4.0 could be attributed to the attachment of *P. catenlannulatus* on GO surface, resulting in the block of reactive sites of GO. The facilitated adsorption at pH > 4.0 was due to the electrostatic attraction of positively charged GO and negatively charged naphthalene at pH > pKa (~9.3). The pH-dependent adsorption further demonstrated that the *P. catenlannulatus* significantly influenced the adsorption of naphthalene on GO.

3.4. Adsorption Isotherms. Figure 4 showed the adsorption isotherms of naphthalene on GO and GO + *P. catenlannulatus*. As illustrated in Figure 4(a), the adsorption of naphthalene on GO obviously increased with increasing naphthalene concentration and then maintained high-level adsorption. However, the adsorption of naphthalene on GO + *P. catenlannulatus* significantly increased with increasing initial naphthalene concentration. The Langmuir and Freundlich models were utilized to fit the adsorption isotherms of naphthalene on GO. The linear forms of Langmuir [35] and Freundlich model [36] can be defined as (5) and (6), respectively:

$$\frac{C_e}{Q_e} = \frac{C_e}{Q_{\max}} + \frac{1}{(K_L \times Q_{\max})}, \quad (5)$$

$$\ln Q_e = \ln K_F + \frac{1}{n} \ln C_e, \quad (6)$$

Table 2: Parameters for Langmuir and Freundlich models of naphthalene adsorption on GO and GO + *P. cateniannulatus*.

Samples	Langmuir model			Freundlich model		
	q_{max} (μg/g)	b (L/mg)	R^2	k_F (mg^{1-n}L^n/g)	$1/n$	R^2
GO	0.167	52.96	0.9997	0.2526	0.131	0.9738
GO + *P. cateniannulatus*	112.3	21.445	0.9582	0.5515	0.279	0.9965

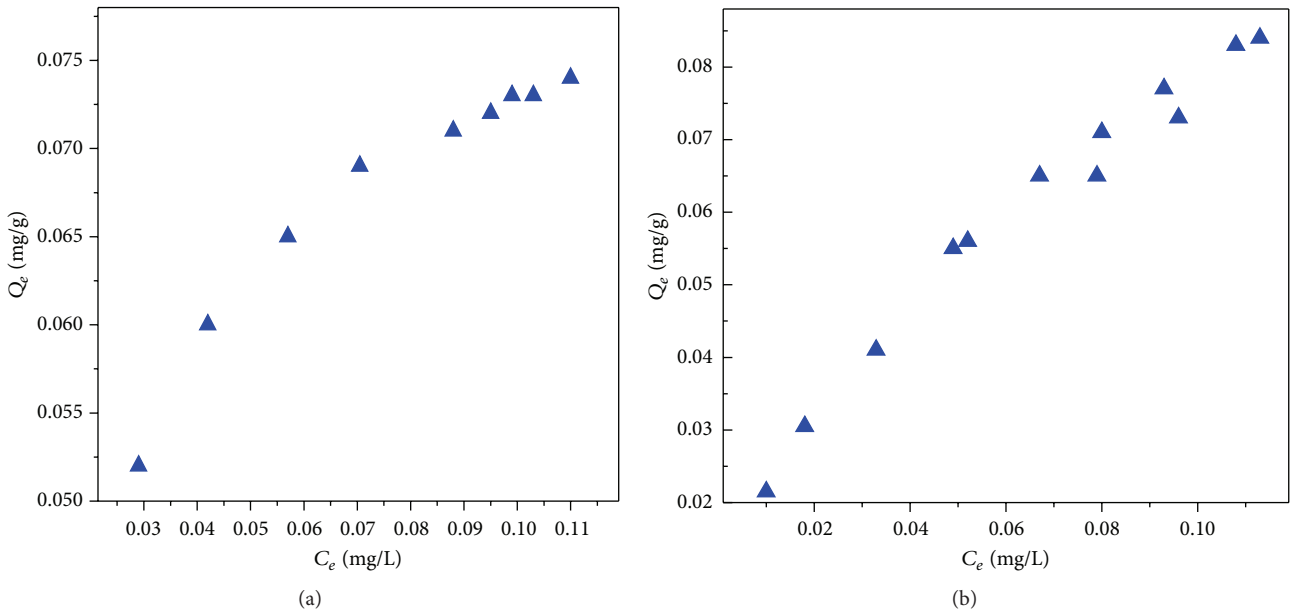

Figure 4: The adsorption isotherms of naphthalene onto GO (a) and GO + *P. cateniannulatus* (b), I = 0.01 mol/L $NaClO_4$, pH 5.0, m/v = 0.25 g/L, and T = 293 K.

where C_e (mg/L) and Q_e (mg/g) are the concentration of naphthalene after equilibrium at solution and solid phase, respectively; K_L (L/mg) and K_F ((mg/g)/(mg/L)$^{1/n}$) are the Langmuir and Freundlich adsorption coefficient, respectively. Q_{max} (mg/g) is maximum adsorption capacity, and $1/n$ is the heterogeneity of the adsorption sites and an indicator of isotherm nonlinearity. The fitted results of naphthalene adsorption on GO and GO + *P. catenlannulatus* were shown in Figure 3 and Table 2. As listed in Table 2, the adsorption of naphthalene on GO can be better fitted by Langmuir model ($R^2 > 0.999$), whereas the adsorption of naphthalene on GO + *P. catenlannulatus* can be satisfactorily simulated by Freundlich model ($R^2 > 0.996$). The maximum adsorption capacities of GO and GO + *P. catenlannulatus* calculated from Langmuir model were 0.167 and 112.3 μg/g for naphthalene at pH 5.0 and 293 K, respectively. The fitted results indicated that the adsorption of naphthalene on GO was attributed to the monolayer adsorption, whereas the high affinity of GO + *P. catenlannulatus* for naphthalene was due to a variety of reactive sites with different adsorption energy. These reactive sites with the different energies were derived from the sieving effect of the powerful groove regions of GO [37], which was further demonstrated by the below characteristic results.

3.5. Adsorption Mechanism. Based on the aforementioned batch adsorption, it was observed that *P. catenlannulatus* significantly influenced the adsorption of naphthalene on GO under various environmental conditions. Therefore, the adsorption mechanism between naphthalene and GO + *P. catenlannulatus* was demonstrated by SEM, TEM, and FTIR techniques. As shown in Figure 1(b), the GO surface became fairly flat and rigid after adsorption. It was also demonstrated from TEM images (Figure 1(d)) that the scrolls on the edge of the GO were mainly unfolded, which was consistent with previous study [13]. The slight accumulation of the GO nanosheets was observed, which indicated the layers tended to aggregate tightly. The surface functional groups of GO nanosheets could form intrasheet bridging; therefore interaction of naphthalene and GO retained a fairly planar geometry because the steric hindrance inhibited the GO nanosheets from wrapping [38]. Therefore, the change in the conformation of GO was responsible to the increased adsorption of naphthalene. Figure 5 showed the FTIR spectra of GO and GO + *P. catenlannulatus* after naphthalene adsorption. For GO, the peaks at approximately 1725, 1620, 1390, and 1085 cm^{-1} corresponded to the stretching vibration of the C=O, skeletal C=C, carboxyl O=C–O, and alkoxy C–O bond, respectively [2, 25, 39, 40]. The widen peaks at 3450 cm^{-1} (data not shown) were assigned to the –OH stretching vibration of adsorbed water [41]. For GO + *P. catenlannulatus*, the peaks of C=C bonds shifted from 1625 to 1633 cm^{-1} after naphthalene adsorption, which indicated that

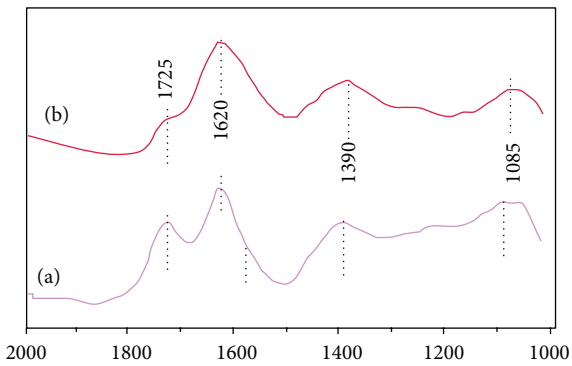

FIGURE 5: FTIR spectra of GO (a) and GO + *P. cateniannulatus* (b) after adsorption of naphthalene.

π-π interactions dominated the adsorption process between GO + *P. catenlannulatus* and naphthalene [4]. The shift of carboxyl O=C–O bending vibration (from 1390 to 1381 cm^{-1}) was greater than that of alkoxy C–O bending vibration (from 1085 to 1079 cm^{-1}), which suggested that high adsorption of naphthalene on GO + *P. catenlannulatus* was attributed to oxygen-containing functional groups of *P. catenlannulatus*, especially –COOH groups. These observations were consistent with previous studies [13, 39].

4. Conclusions

The effect of *P. catenlannulatus* on the adsorption of naphthalene on GO was investigated by batch techniques. Based on the characteristic results, it was demonstrated that GO nanosheets presented a variety of oxygen-containing functional groups such as epoxy, carboxyl, carbonyl, and hydroxyl groups. The adsorption kinetics indicated that the adsorption of naphthalene on GO and GO + *P. catenlannulatus* can be satisfactorily fitted pseudo-first-order and pseudo-second-order kinetic model, respectively. The pH-dependent adsorption showed that the high-level adsorption of naphthalene on GO + *P. catenlannulatus* was observed at pH 5.0–6.0; then adsorption of naphthalene on GO + *P. catenlannulatus* slightly decreased at pH > 6.5. It was observed that *P. catenlannulatus* inhibited the adsorption of naphthalene on GO at pH < 4.0, whereas the increased adsorption was observed at pH > 4.0. The adsorption of naphthalene on GO and GO + *P. catenlannulatus* can be better fitted by Langmuir and Freundlich model, respectively. According to the SEM and TEM analysis after adsorption, the change in the conformation of GO was responsible to the increased adsorption of naphthalene. The GO surface became fairly flat and rigid after adsorption. It was also demonstrated from TEM images that the scrolls on the edge of the GO were mainly unfolded. According to FTIR analysis, naphthalene was absorbed by oxygen-containing functional groups of GO, especially –COOH groups. The finding in the study provides the implication for the preconcentration and removal of polycyclic aromatic hydrocarbons from environment cleanup applications.

Conflict of Interests

The authors declare that there is no conflict of interests regarding the publication of this paper.

Acknowledgment

Financial support from 2012 Annual National Forestry Public Welfare Industry Research Projects (no. 201304407) is acknowledged.

References

[1] A. K. Geim and K. S. Novoselov, "The rise of graphene," *Nature Materials*, vol. 6, no. 3, pp. 183–191, 2007.

[2] Y. Sun, Q. Wang, C. L. Chen, X. K. Tan, and X. Wang, "Interaction between Eu(III) and graphene oxide nanosheets investigated by batch and extended X-ray absorption fine structure spectroscopy and by modeling techniques," *Environmental Science and Technology*, vol. 46, no. 11, pp. 6020–6027, 2012.

[3] Y. B. Sun, S. B. Yang, Y. Chen, C. C. Ding, W. C. Cheng, and X. K. Wang, "Adsorption and desorption of U(VI) on functionalized graphene oxides: a combined experimental and theoretical study," *Environmental Science & Technology*, vol. 49, no. 7, pp. 4255–4262, 2015.

[4] G. K. Ramesha, A. V. Kumara, H. B. Muralidhara, and S. Sampath, "Graphene and graphene oxide as effective adsorbents toward anionic and cationic dyes," *Journal of Colloid and Interface Science*, vol. 361, no. 1, pp. 270–277, 2011.

[5] F. Liu, S. Chung, G. Oh, and T. S. Seo, "Three-dimensional graphene oxide nanostructure for fast and efficient water-soluble dye removal," *ACS Applied Materials and Interfaces*, vol. 4, no. 2, pp. 922–927, 2012.

[6] J. N. Tiwari, K. Mahesh, N. H. Le et al., "Reduced graphene oxide-based hydrogels for the efficient capture of dye pollutants from aqueous solutions," *Carbon*, vol. 56, pp. 173–182, 2013.

[7] P. N. Diagboya, B. I. Olu-Owolabi, D. Zhou, and B.-H. Han, "Graphene oxide-tripolyphosphate hybrid used as a potent sorbent for cationic dyes," *Carbon*, vol. 79, no. 1, pp. 174–182, 2014.

[8] Q. Wang, J. X. Li, Y. Song, and X. K. Wang, "Facile synthesis of high-quality plasma-reduced graphene oxide with ultrahigh 4,4′-dichlorobiphenyl adsorption capacity," *Chemistry—An Asian Journal*, vol. 8, no. 1, pp. 225–231, 2013.

[9] S. Zeng, N. Gan, R. Weideman-Mera, Y. Cao, T. Li, and W. Sang, "Enrichment of polychlorinated biphenyl 28 from aqueous solutions using Fe_3O_4 grafted graphene oxide," *Chemical Engineering Journal*, vol. 218, pp. 108–115, 2013.

[10] B. Beless, H. S. Rifai, and D. F. Rodrigues, "Efficacy of carbonaceous materials for sorbing polychlorinated biphenyls from aqueous solution," *Environmental Science and Technology*, vol. 48, no. 17, pp. 10372–10379, 2014.

[11] L. L. Ji, W. Chen, Z. Y. Xu, S. R. Zheng, and D. Q. Zhu, "Graphene nanosheets and graphite oxide as promising adsorbents for removal of organic contaminants from aqueous solution," *Journal of Environmental Quality*, vol. 42, no. 1, pp. 191–198, 2013.

[12] Y. B. Sun, S. B. Yang, G. X. Zhao, Q. Wang, and X. K. Wang, "Adsorption of polycyclic aromatic hydrocarbons on graphene oxides and reduced graphene oxides," *Chemistry—an Asian Journal*, vol. 8, no. 11, pp. 2755–2761, 2013.

[13] J. Wang, Z. M. Chen, and B. L. Chen, "Adsorption of polycyclic aromatic hydrocarbons by graphene and graphene oxide nanosheets," *Environmental Science and Technology*, vol. 48, no. 9, pp. 4817–4825, 2014.

[14] J. Zhao, Z. Wang, J. C. White, and B. Xing, "Graphene in the aquatic environment: adsorption, dispersion, toxicity and transformation," *Environmental Science and Technology*, vol. 48, no. 17, pp. 9995–10009, 2014.

[15] F. B. Li, Z. M. Gao, X. Y. Li, and L. J. Fang, "The effect of *Paecilomyces catenlannulatus* on removal of U(VI) by illite," *Journal of Environmental Radioactivity*, vol. 137, pp. 31–36, 2014.

[16] R. Selvakumar, S. Kavitha, M. Sathishkumar, V. Jayavignesh, and K. Swaminathan, "Liquid phase separation of As(V) from aqueous solution using pretreated paecilomyces variotii biomass," *Separation Science and Technology*, vol. 45, no. 6, pp. 776–785, 2010.

[17] S. S. Ahluwalia and D. Goyal, "Removal of Cr(VI) from aqueous solution by fungal biomass," *Engineering in Life Sciences*, vol. 10, no. 5, pp. 480–485, 2010.

[18] S. Sharma and A. Adholeya, "Detoxification and accumulation of chromium from tannery effluent and spent chrome effluent by *Paecilomyces lilacinus* fungi," *International Biodeterioration and Biodegradation*, vol. 65, no. 2, pp. 309–317, 2011.

[19] M. Słaba and J. Długoński, "Efficient Zn^{2+} and Pb^{2+} uptake by filamentous fungus *Paecilomyces marquandii* with engagement of metal hydrocarbonates precipitation," *International Biodeterioration and Biodegradation*, vol. 65, no. 7, pp. 954–960, 2011.

[20] F. B. Li, Z. M. Gao, X. Y. Li, and L. J. Fang, "The adsorption of U(VI) and Hg(II) on *Paecilomyces catenlannulatus* proteases," *Journal of Radioanalytical and Nuclear Chemistry*, vol. 298, no. 3, pp. 2043–2047, 2013.

[21] F. B. Li, Z. M. Gao, X. Y. Li, and L. J. Fang, "The effect of environmental factors on the uptake of ^{60}Co by *Paecilomyces catenlannulatus*," *Journal of Radioanalytical and Nuclear Chemistry*, vol. 299, no. 3, pp. 1281–1286, 2014.

[22] W. S. Hummers and R. E. Offeman, "Preparation of graphitic oxide," *Journal of the American Chemical Society*, vol. 80, no. 6, p. 1339, 1958.

[23] Y. B. Sun, C. L. Chen, D. D. Shao et al., "Enhanced adsorption of ionizable aromatic compounds on humic acid-coated carbonaceous adsorbents," *RSC Advances*, vol. 2, no. 27, pp. 10359–10364, 2012.

[24] Y. B. Sun, C. L. Chen, X. L. Tan et al., "Enhanced adsorption of Eu(III) on mesoporous Al_2O_3/expanded graphite composites investigated by macroscopic and microscopic techniques," *Dalton Transactions*, vol. 41, no. 43, pp. 13388–13394, 2012.

[25] Y. B. Sun, D. D. Shao, C. L. Chen, S. B. Yang, and X. K. Wang, "Highly efficient enrichment of radionuclides on graphene oxide-supported polyaniline," *Environmental Science and Technology*, vol. 47, no. 17, pp. 9904–9910, 2013.

[26] R. L. D. Whitby, V. M. Gun'ko, A. Korobeinyk et al., "Driving forces of conformational changes in single-layer graphene oxide," *ACS Nano*, vol. 6, no. 5, pp. 3967–3973, 2012.

[27] Z. X. Jin, X. X. Wang, Y. B. Sun, Y. J. Ai, and A. K. Wang, "Adsorption of 4-n-nonylphenol and bisphenol-A on magnetic reduced graphene oxides: a combined experimental and theoretical studies," *Environmental Science & Technology*, vol. 49, no. 15, pp. 9168–9175, 2015.

[28] Y. B. Sun, S. B. Yang, C. C. Ding, W. C. Cheng, and Z. X. Jin, "Tuning the chemistry of graphene oxides by a sonochemical approach: application of adsorption properties," *RSC Advances*, vol. 5, no. 32, pp. 24886–24892, 2015.

[29] C. C. Ding, W. C. Cheng, Y. B. Sun, and X. K. Wang, "Effects of *Bacillus subtilis* on the reduction of U(VI) by nano-Fe^0," *Geochimica et Cosmochimica Acta*, vol. 165, pp. 86–107, 2015.

[30] Y. B. Sun, C. C. Ding, W. C. Cheng, and X. K. Wang, "Simultaneous adsorption and reduction of U(VI) on reduced graphene oxide-supported nanoscale zerovalent iron," *Journal of Hazardous Materials*, vol. 280, pp. 399–408, 2014.

[31] M.-C. Hsiao, S.-H. Liao, M.-Y. Yen et al., "Preparation of covalently functionalized graphene using residual oxygen-containing functional groups," *ACS Applied Materials and Interfaces*, vol. 2, no. 11, pp. 3092–3099, 2010.

[32] S. Stankovich, D. A. Dikin, R. D. Piner et al., "Synthesis of graphene-based nanosheets via chemical reduction of exfoliated graphite oxide," *Carbon*, vol. 45, no. 7, pp. 1558–1565, 2007.

[33] S. Lagergren, "Zur theorie der sogenannten adsorption geloster stoffe," *Kungliga Svenska Vetenskapsakademiens Handlingar*, vol. 24, pp. 1–39, 1989.

[34] Y. S. Ho and G. McKay, "Pseudo-second order model for sorption processes," *Process Biochemistry*, vol. 34, no. 5, pp. 451–465, 1999.

[35] I. Langmuir, "The adsorption of gases on plane surfaces of glass, mica and platinum," *Journal of the American Chemical Society*, vol. 40, no. 9, pp. 1361–1403, 1918.

[36] H. M. F. Freundlich, "Uber die adsorption in Losungen," *The Journal of Physical Chemistry*, vol. 57, pp. 385–470, 1906.

[37] P. Lazar, F. Karlický, P. Jurecka et al., "Adsorption of small organic molecules on graphene," *Journal of the American Chemical Society*, vol. 135, no. 16, pp. 6372–6377, 2013.

[38] R. L. D. Whitby, A. Korobeinyk, S. V. Mikhalovsky, T. Fukuda, and T. Maekawa, "Morphological effects of single-layer graphene oxide in the formation of covalently bonded polypyrrole composites using intermediate diisocyanate chemistry," *Journal of Nanoparticle Research*, vol. 13, no. 10, pp. 4829–4837, 2011.

[39] J. Y. Huang, Z. W. Wu, L. W. Chen, and Y. B. Sun, "Surface complexation modeling of adsorption of Cd(II) on graphene oxide," *Journal of Molecular Liquids*, vol. 209, pp. 753–758, 2015.

[40] C. C. Ding, W. C. Cheng, Y. B. Sun, and X. K. Wang, "Determination of chemical affinity of graphene oxide nanosheets with radionuclides investigated by macroscopic, spectroscopic and modeling techniques," *Dalton Transactions*, vol. 43, no. 10, pp. 3888–3896, 2014.

[41] Y. B. Sun, J. X. Li, and X. K. Wang, "The retention of uranium and europium onto sepiolite investigated by macroscopic, spectroscopic and modeling techniques," *Geochimica et Cosmochimica Acta*, vol. 140, pp. 621–643, 2014.